WARSAW UNIVERSITY OF TECHNOLOGY Index 351733
FACULTY OF CIVIL ENGINEERING
COMMITTEE FOR CIVIL AND WATER ENGINEERING
POLISH ACADEMY OF SCIENCES ISSN 1230-2945

DOI: 10.24425/ace.2020.134400
ARCHIVES OF CIVIL ENGINEERING
Vol. LXVI ISSUE 3 2020

3D ABAQUS SIMULATION OF BENT SOFTWOOD ELEMENTS

B. KAWECKI[1], J. PODGÓRSKI[2]

The article presents research on modelling fracture in softwood bent elements. This kind of timber is the one most exploited for construction. Authors present a brief review on the subject with emphasis on three basic attempts: Linear Elastic Fracture Mechanics (LEFM), Continuum Damage Mechanics (CDM) and Hill's Function (HF). Proposed 3D solution bases on Hill's Function applied in the ABAQUS FEM code. The new idea includes isolating theoretical compression and tension zones in a model. Then, it is possible to distinguish between compressive and tensile strength and predict a real behaviour of bent elements. Introducing general dependencies between material properties leads to the need of determining only longitudinal elastic modulus (E_L) and modulus of rupture (MOR). It is practical because these parameters are the main reported in a scientific and technical literature. Authors describe all of the assumptions in details. The experimental tests and Digital Image Correlation method (DIC) validate the FEM model.

Keywords: FEM, Wood Modelling, Softwood, Fracture, Destruction

[1]MSc., Lublin University of Technology, Faculty of Civil Engineering and Architecture, ul. Nadbystrzycka 40, 20-618 Lublin, Poland, e-mail: b.kawecki@pollub.pl
[2]Prof., Lublin University of Technology, Faculty of Civil Engineering and Architecture, ul. Nadbystrzycka 40, 20-618 Lublin, Poland, e-mail: j.podgorski@pollub.pl

1. INTRODUCTION

Literature describes a nonlinear behaviour of timber with three main concepts. The first is the LEFM (Linear Elastic Fracture Mechanics). Basic material properties regulating the fracture process are critical stress intensity factor (fracture toughness) and energy release rate in corresponding modes (Fig. 1).

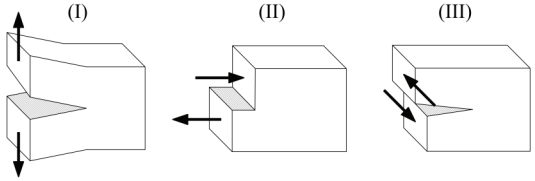

Fig. 1. Basic modes of fracture.

Silva [1] and Kossakowski [2, 3] carry out numerical analyses of DCB (Double Cantilever Beam) and ENF (End Notched Flexure) test (Fig. 2). They calculate energy release rate in mode I and II (G_{Ic} and G_{IIc}) for pinewood. Experimental determination of fracture toughness and energy release rate in timber is also a subject of other finds, for example done by Prokopski [4] or Yoshikara [5].

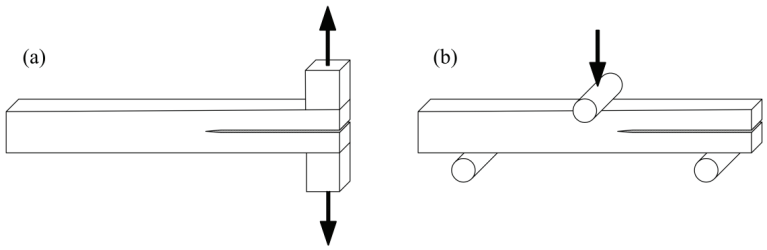

Fig. 2. (a) DCB – Double Cantilever Beam, (b) ENF – End Notched Flexure.

Stanzl-Tschegg [6] and Vasic [7] propose a WS (Wedge-Splitting) sample for testing a fracture in mode I (Fig. 3a). The value of G_{Ic} they measure is comparable to this presented by Kossakowski [3]. Fortino [8] adds cohesive elements to the WS sample on the expected crack path. He gets a good agreement with Stanzl-Tschegg [6] experimental results.

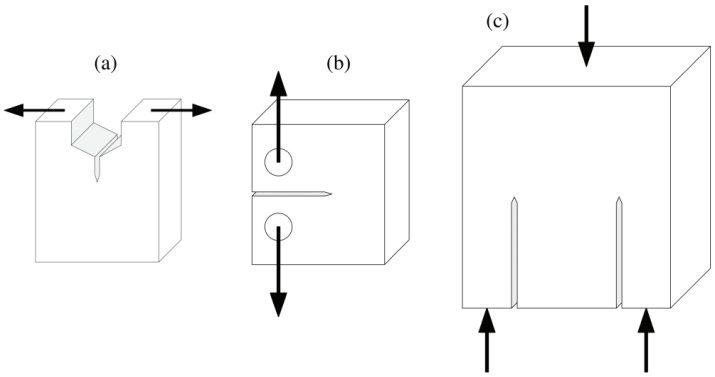

Fig. 3. (a) WS – Wedge Splitting sample, (b) K_{Ic} specimen, (c) K_{IIc} specimen.

Qiu [9, 10] presents a different concept. He calculates the fracture toughness K_{Ic} and K_{IIc} from the standard specimens (Fig. 3 b,c). Then, creates FEM model using XFEM (Extended Finite Element) method, which gives results close to laboratory tests.

The second modelling approach is CDM (Continuum Damage Mechanics). Constitutive law is bilinear and includes softening. It makes possible to distinguish material properties in different directions and depending on a stress state (compression, tension). Sandhaas [11] proposes a 3D model, in which he takes into account plastic behaviour in compression and brittle in tension. Nine different material degradation parameters control a fracture development. Their calculation bases on the introduced fracture energy in a respective direction. Orlando [12] uses the Sandhaas' model to predict a damage process in wooden girders cut in selected places and repaired with glued rods. Khorsandnia [13] and Valipour [14] propose a 2D model based on Hashin's criterion. It provides a bilinear material characteristic with a distinction between compression and tension. The authors examine full and I-beam girders with holes or cuts and get consistency of results.

The third concept is HF (Hill's Function), representing an anisotropic plastic flow after reaching a yield point. General advantages and disadvantages of using the criterion describe Mascia and Simoni [15]. Oudjene and Khelifa [16, 17] consider a compression of cuboidal samples parallel to grains and validate the FEM model based on Reiterer and Stanzl-Tschegg experiments [18]. Later, they expand it to the sample with a circular hole and steel dowel (Fig. 4a). Simulations cause timber to crush in a contact zone. Pranata [19] and Santos [20] build a 3D model and change the orientation of fibres. This time, grains of adjacent elements are perpendicular to each other. Because of the arrangement the dowel presses the components both along and across the fibres

(Fig. 4b). This is a more complex situation than in the case of preceding study. To predict a crack, the authors add a cohesive surface on the expected fracture path.

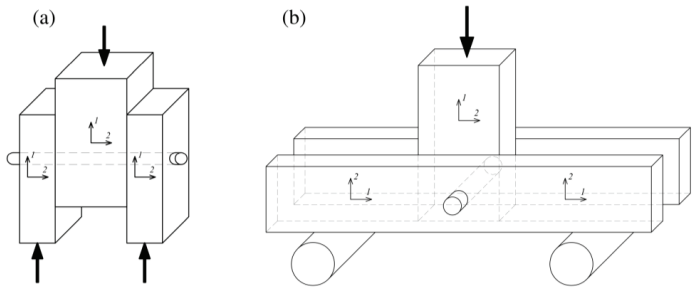

Fig. 4. (a) Oudjene specimen, (b) Santos specimen.

Summarising, a 3D solution for modelling wood, which incorporates sufficient complexity is Hill's Function. The advantages are a fast convergence of computations and simple implementation of required parameters. Despite this, the model needs a general enrichment to well represent stress state in bending. The authors present the assumptions in the following part of the article.

2. DESCRIPTION OF THE MODEL

Wood is an orthotropic material. Constitutive relation determining a linear-elastic behaviour in a 3D space is:

$$\begin{bmatrix} \varepsilon_{11} \\ \varepsilon_{22} \\ \varepsilon_{33} \\ \gamma_{12} \\ \gamma_{13} \\ \gamma_{23} \end{bmatrix} = \begin{bmatrix} \frac{1}{E_1} & -\frac{\nu_{21}}{E_2} & -\frac{\nu_{31}}{E_3} & 0 & 0 & 0 \\ -\frac{\nu_{12}}{E_1} & \frac{1}{E_2} & -\frac{\nu_{32}}{E_3} & 0 & 0 & 0 \\ -\frac{\nu_{13}}{E_1} & -\frac{\nu_{23}}{E_2} & \frac{1}{E_3} & 0 & 0 & 0 \\ 0 & 0 & 0 & \frac{1}{G_{12}} & 0 & 0 \\ 0 & 0 & 0 & 0 & \frac{1}{G_{13}} & 0 \\ 0 & 0 & 0 & 0 & 0 & \frac{1}{G_{23}} \end{bmatrix} \begin{bmatrix} \sigma_{11} \\ \sigma_{22} \\ \sigma_{33} \\ \tau_{12} \\ \tau_{13} \\ \tau_{23} \end{bmatrix} \tag{2.1}$$

ABAQUS FEM code [21] allows applying the Hill's function to represent an anisotropic plastic flow of a material after reaching a yield point. The function is:

$$f(\sigma)=\sqrt{F(\sigma_{22}-\sigma_{33})^2+G(\sigma_{33}-\sigma_{11})^2+H(\sigma_{11}-\sigma_{22})^2+2L\tau_{23}^{\ 2}+2M\tau_{31}^{\ 2}+2N\tau_{12}^{\ 2}} \tag{2.2}$$

where:

$$F=\frac{1}{2}\left(\frac{1}{R_{22}^{\ 2}}+\frac{1}{R_{33}^{\ 2}}-\frac{1}{R_{11}^{\ 2}}\right) \qquad G=\frac{1}{2}\left(\frac{1}{R_{33}^{\ 2}}+\frac{1}{R_{11}^{\ 2}}-\frac{1}{R_{22}^{\ 2}}\right) \tag{2.3}$$

$$H=\frac{1}{2}\left(\frac{1}{R_{11}^{\ 2}}+\frac{1}{R_{22}^{\ 2}}-\frac{1}{R_{33}^{\ 2}}\right) \qquad L=\frac{3}{2R_{23}^{\ 2}} \qquad M=\frac{3}{2R_{13}^{\ 2}} \qquad N=\frac{3}{2R_{12}^{\ 2}} \tag{2.5}$$

Because Hill's Function does not distinguish between compressive and tensile strength, we propose a theoretical separation of compression and tension zones (Fig. 5).

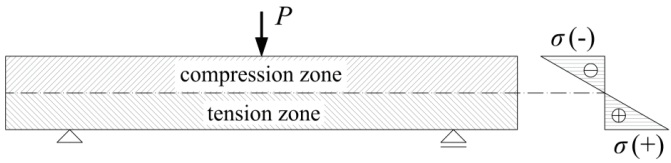

Fig. 5. Theoretical isolation of the compression and tension zones.

After making this assumption, the constitutive law is (Fig. 6):

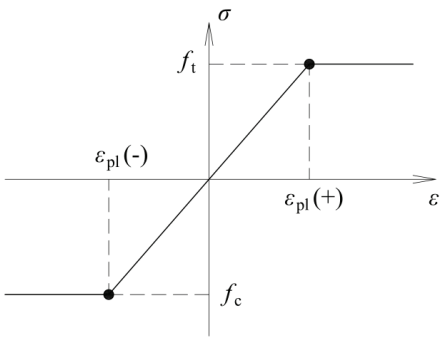

Fig. 6. Constitutive law for wood used in the model.

3. LABORATORY TESTS AND NUMERICAL SIMULATIONS

The initial step is preparing 10 specimens of pinewood with dimensions of 19×45×500 mm. All are cut from the same batch of softwood, dried to 16-18% of moisture content. Knots and other defects are neglected to get as homogenous timber structure as possible. During preparation and testing the samples, a relative air humidity is on the level of 60%. Fig. 7 shows a simplified pattern for defining axes for a 3D orthotropic model. In the illustration there is also visible a typical sample with two surfaces painted with a special gradient. In the front and bottom surface it is possible to examine the method of destruction compared to the FEM model. The testing machine is MTS 809. An additional equipment used for measurements is the ARAMIS system, based on Digital Image Correlation (DIC).

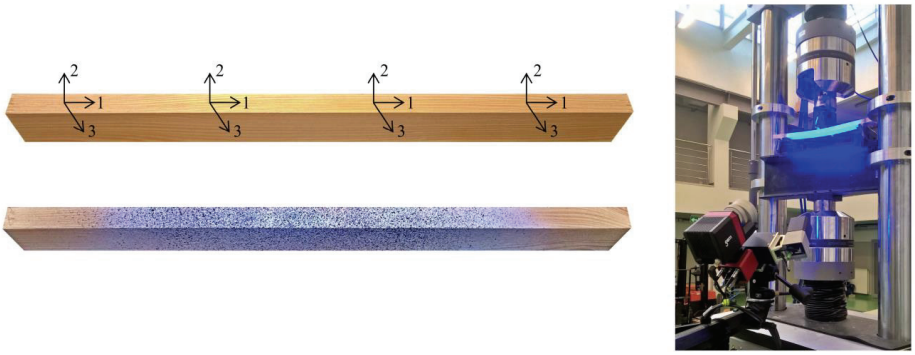

Fig. 7. A typical sample and the laboratory setup.

Because wood is a material tested all over the world, a procedure of selection of the parameters for modelling should include using properties from the literature. The example of such a position may be Wood Handbook [22]. Modulus of elasticity along the fibres is determined based on measuring the deflection of the bottom of the beam. Even in the orthotropic model, the longitudinal modulus of elasticity has the biggest impact on deflection.

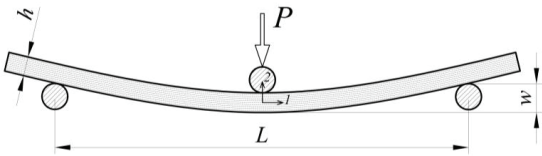

Fig. 8. Denotations for a three point bending test.

The value of the displacement of the middle point of the beam in a three point bending (Fig. 8) determines the formula:

$$w = \frac{PL^3}{48E_1 J} + \frac{PL}{4G_{12}A'} \tag{3.1}$$

where:

$A' = \frac{5}{6}bh$ - modified rectangular cross-sectional area

$G_{12} = \frac{E_1}{16}$ - shear modulus depending on the longitudinal modulus

$J = \frac{bh^3}{12}$ - moment of inertia of the rectangular section

After substituting all the variables, we get an equation that allows calculating the deflection value depending only on the longitudinal modulus of elasticity. From laboratory tests it is feasible to get *P/w* rate in the linear-elastic range, and thus the values of the longitudinal modulus of elasticity:

$$E_1 = \frac{P}{w}\left(\frac{L^3}{4bh^3} + \frac{24L}{5bh}\right) \tag{3.2}$$

Aramis system measures deflection (w) at the bottom of the beam, while MTS machine records the applied force (P). Calculation of other elastic parameters relates to Wood Handbook [22] and Kossakowski [2, 3]. In the both sources relations between elastic parameters are similar:

$$E_1 : E_2 : E_3 = 25 : 1.6 : 1 \tag{3.3}$$

$$G_{12} : G_{13} : G_{23} = 10.4 : 7.7 : 1 \tag{3.4}$$

Poisson's coefficients base on average values and are equal: ν_{12}=0.335, ν_{13}=0.358, ν_{23}=0.416. Another parameter specified in the literature is tensile strength in bending, often called the modulus of rupture (MOR), calculated according to a simple formula from the theory of elasticity:

$$f_{t,1} = \frac{3}{2}\frac{P_{\max}L}{bh^2} \tag{3.5}$$

The authors point out that the remaining strengths depend on the tensile strength along the fibres. Based on the parameters marked in Wood Handbook [22], the dependencies are forming as the trend lines show (Fig. 9):

$$f_{c,1} = 0.513 \cdot f_{t,1} + 3.480 \tag{3.6}$$

$$f_{c,2} = 0.075 \cdot f_{t,1} - 0.865 \tag{3.7}$$

$$f_{v,12} = 0.083 \cdot f_{t,1} + 2.272 \tag{3.8}$$

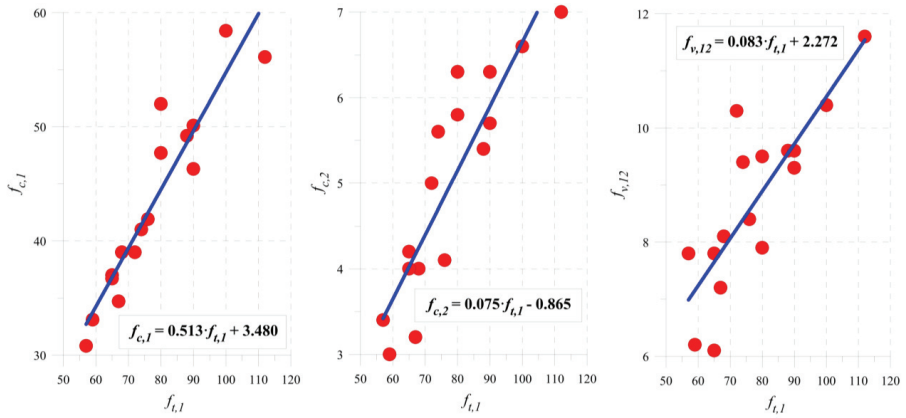

Fig. 9. Trend lines of the strengths determined based on laboratory tests.

Table 1. Elastic parameters and strengths of the tested softwood.

Sample number	E_1 [GPa]	E_2 [GPa]	E_3 [GPa]	G_{12} [GPa]	G_{13} [GPa]	G_{23} [GPa]	$f_{t,1}$ [MPa]	$f_{c,1}$ [MPa]	$f_{c,2}$ [MPa]	$f_{v,12}$ [MPa]
1	11.574	0.741	0.463	0.723	0.536	0.070	92.91	51.05	6.10	9.89
2	15.955	1.021	0.638	0.997	0.738	0.096	109.29	59.44	7.33	11.23
3	15.089	0.966	0.604	0.943	0.698	0.091	88.41	48.74	5.77	9.52
4	15.576	0.997	0.623	0.974	0.721	0.094	91.83	50.50	6.02	9.80
5	15.738	1.007	0.630	0.984	0.728	0.095	92.5	50.84	6.07	9.86
6	16.874	1.080	0.675	1.055	0.781	0.101	101.74	55.57	6.77	10.61
7	15.955	1.021	0.638	0.997	0.738	0.096	100.42	54.89	6.67	10.51
8	17.199	1.101	0.688	1.075	0.796	0.103	103.77	56.61	6.92	10.78
9	14.873	0.952	0.595	0.930	0.688	0.089	94.81	52.02	6.25	10.05
10	13.413	0.858	0.537	0.838	0.621	0.081	82.69	45.82	5.34	9.05
AVG	**15.225**	**0.974**	**0.609**	**0.952**	**0.705**	**0.091**	**95.84**	**52.55**	**6.32**	**10.13**

Elastic parameters and strengths summarises Table 1. Because the proposed model does not distinguish between compressive and tensile strength and they are close to each other, we assume that $f_{t,2} = f_{c,2}$. In addition, parameters for axis (2) and (3) are equal $f_{c,2} = f_{c,3}$ and shear strength

is identical in each direction $f_{v,12} = f_{v,13} = f_{v,23}$. In the next step, we calculate the parameters required in the dependencies 2.2-2.6 of Hill's Function. The reference value for all of them is the bending tensile strength $f_{t,1}$. $R_{11}(+)$ means the coefficient used in the tension, while $R_{11}(-)$ in the compression zone. Parameter λ calibrates the strength in the tension region. We use the formulas:

$$R_{11}(+) = \frac{\lambda f_{t,1}}{f_{t,1}} \qquad R_{11}(-) = \frac{f_{c,1}}{f_{t,1}} = 0.548 \qquad R_{22} = R_{33} = \frac{f_{c,2}}{f_{t,1}} = 0.066 \tag{3.9}$$

$$R_{12} = R_{13} = R_{23} = \frac{\sqrt{3} f_{v,12}}{f_{t,1}} = 0.183 \tag{3.10}$$

The 6th polynomial represents each of the experimental force-deflection curve (P/w). This statistical approximation enables to mark the same points on a diagram, as calculated in the FEM model. Fig. 11a presents results from testing machine, average ultimate force and its average deviation. However, Fig. 11b shows the experimental average curve and a deviation envelope according to the 6th polynomial representation.

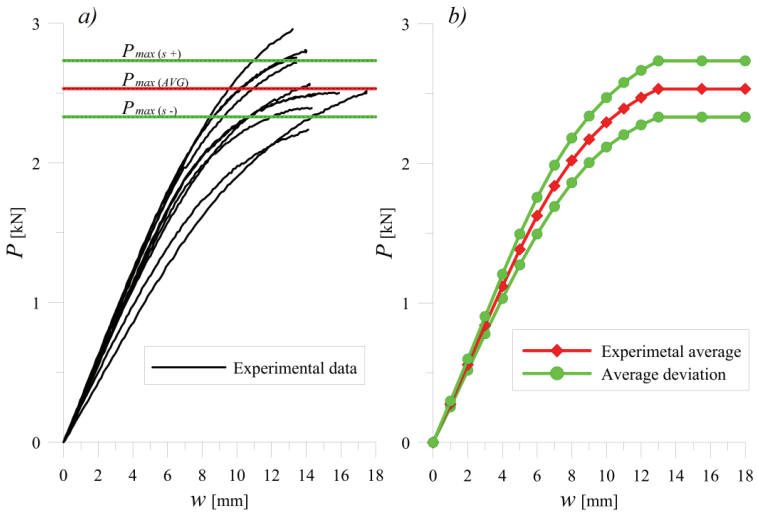

Fig. 10. Experimental P/w curves and its statistical approximations

In a numerical modelling, it is crucial to choose finite elements which behave well in a complex stress state. Hemanth [23] studies all the 3D elements, which are available in the ABAQUS FEM

code. He concludes that the finest are 20-node elements with 27 integration points, named C3D20. They are numerically expensive, but produce physical results in bending and stress concentration areas. The amount of four C3D20 members at the height of the bent sample gives results identical to the analytical solutions. Fig. 11 shows the finite element mesh and boundary conditions:

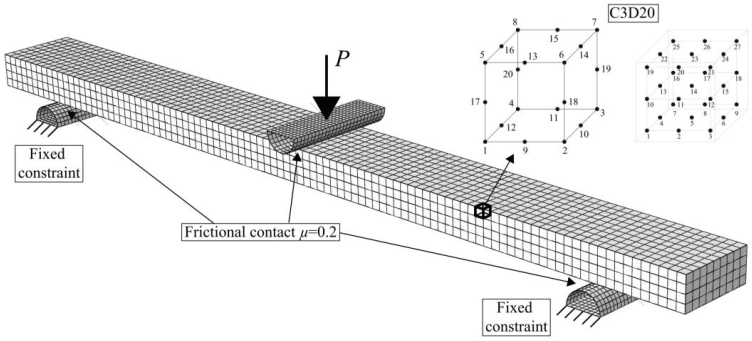

Fig. 11. Finite element mesh and boundary conditions used in the analyses.

Based on the investigations, we claim that the model reflects the stiffness of the real system in the linear-elastic range (K_u). For the FEM model it is K_u = 0.285 kN/mm and for the real samples K_u = 0.282 kN/m. It approves the correctness of the selected parameters for an elastic modelling.

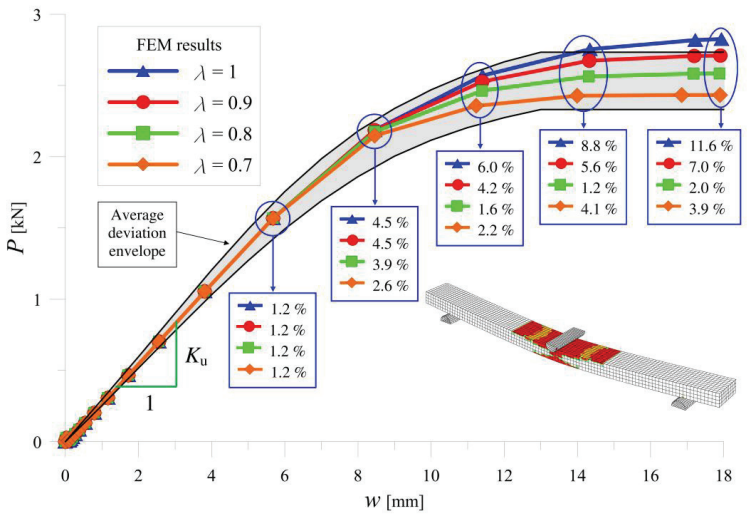

Fig. 12. Comparison of *P/w* relation from FEM model and laboratory tests.

However, we should calibrate the material in the FEM model to get the maximum force from laboratory experiments. For this purpose, we introduce the parameter λ changing tensile strength in the tension zone (formula 3.9). Calculations continue until the entire cross-section plasticises. The results of the maximum force got for most of the values are within the standard deviation of laboratory tests. A graph in Fig. 12 shows the numerical simulations related to laboratory tests. Frames in the marked points collect average errors for each value of λ. The most-matched results gives λ=0.8.

Therefore, we analyse the behaviour of the wooden beam in the non-elastic range and compare to the way of destruction achieved in experiments. Fig. 13 shows a comparison of plasticised zones from the FEM model (red) with zones of experimental gradient destruction because of stretching (yellow). We can notice that cracking of the wood in the tension zone does not occur in one point in the middle of the sample, but spread over a larger area. The proposed numerical model captures this behaviour well.

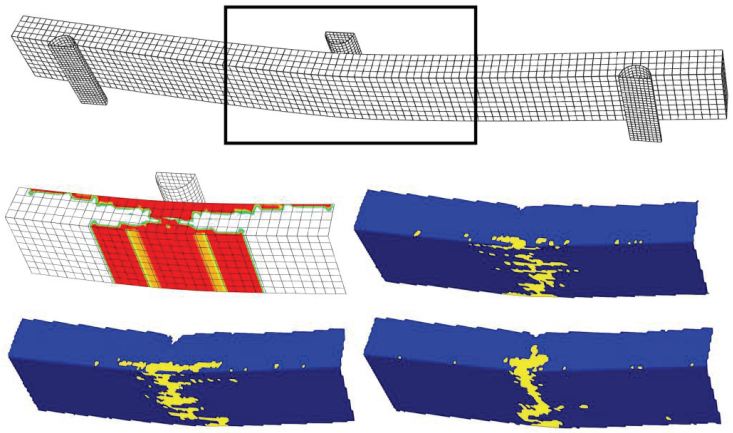

Fig. 13. Comparison of forms of destruction from the FEM model and laboratory tests.

4. CONCLUSIONS

In summary, numerical modelling of wood is a complex process. There are no models in the literature regarding progressive damage that allow analysis of any kind of structure. Researchers calibrate each model depending on the expected stress state and the way of destruction.

The authors plan to use the model to predict a behaviour of wood-based composite bent girders, where, for example, a delamination of several bonded surfaces occurs as simultaneous. It leads to the desire of a solution for wood which is stable and incorporates a sufficient complexity. Amount of parameters and problems with convergence of the calculations in Hill's Function are much smaller than in case of other methods found in the literature. It is worth to point out the very practical aspect, as direct availability of the material model in ABAQUS FEM code.

The method presented in the paper enables modelling wood elements in a 3D state when bending. Theoretical isolation of the compression and tension zones enrich the solution. It allows to distinguish between different strengths of wood in each stress state. The FEM model represents both plastic flow in a middle stage of compression and maximum force prediction because of tension. Force-deflection response is comparable to a physical behaviour of the elements.

Considering all the above, we can state that we may use the model in a further research, after a proper calibration.

ACKNOWLEDGEMENTS: Research presented in the paper was supported by science financing subsidy Lublin university of technology fn16/ilt/2020.

REFERENCES

1. M. A. L. Silva, M. F. S. F. de Moura, J. J. L. Morais, "Numerical analysis of the ENF test for mode II wood fracture", Composites Part A: Applied Science and Manufacturing, 37 (9), pp. 1334–1344, 2006.
2. P. G. Kossakowski, "Influence of anisotropy on the energy release rate GI for highly orthotropic materials", Journal of Theoretical and Applied Mechanics, 45 (4), pp. 739–752, 2007.
3. P. G. Kossakowski, "Fracture toughness of pine wood for I and II loading modes", Archives of Civil Engineering, 54 (3), pp. 509–529, 2008.
4. G. Prokopski, "Investigation of wood fracture toughness using mode II fracture (shearing)", Journal of Materials Science, 30 (18), pp. 4745–4750, 1995.
5. H. Yoshihara, M. Ohta, "Measurement of mode II fracture toughness of wood by the end-notched flexure test", Journal of Wood Science, 46 (4), pp. 273–278, 2000.
6. S. Stanzl-Tschegg, D.-M. Tan, E. Tschegg, "New splitting method for wood fracture characterization", Wood Science and Technology, 29 (1), pp. 31–50, 1995.
7. S. Vasic, S. Stanzl-Tschegg, "Experimental and numerical investigation of wood fracture mechanisms at different humidity levels", Holzforschung, 61 (4), pp. 367–374, 2007.
8. S. Fortino, G. Zagari, A. L. Mendicino, G. Dill-Langer, "A simple approach for FEM simulation of Mode I cohesive crack growth in glued laminated timber under short-term

loading", Rakenteiden Mekaniikka (Journal of Structural Mechanics), 45 (1), pp. 1–20, 2012.
9. L. P. Qiu, E. C. Zhu, H. Z. Zhou, L. Y. Liu, "Fracture Toughness of Northeast China Larch", Key Engineering Materials, 517, pp. 661–668, 2012.
10. L. P. Qiu, E. C. Zhu, J. W. G. van de Kuilen, "Modeling crack propagation in wood by extended finite element method", European Journal of Wood and Wood Products, 72 (2), pp. 273–283, 2014.
11. C. Sandhaas, J. W. G. van de Kuilen, "Material model for wood", Heron Special Issue: Timber modelling, 58 (2/3), 2013.
12. N. Orlando, Y. Taddia, E. Benvenuti, B. Pizzo, C. Alessandri, "End-repair of timber beams with laterally-loaded glued-in rods: Experimental trials and failure prediction through modelling", Construction and Building Materials, 195, pp. 623–637, 2019.
13. N. Khorsandnia, H. R. Valipour, K. Crews, "Nonlinear finite element analysis of timber beams and joints using the layered approach and hypoelastic constitutive law", Engineering Structures, 46, pp. 606–614, 2013.
14. H. Valipour, N. Khorsandnia, K. Crews, S. Foster, "A simple strategy for constitutive modelling of timber", Construction and Building Materials, 53, pp. 138–148, 2014.
15. N. T. Mascia, R. A. Simoni, "Analysis of failure criteria applied to wood", Engineering Failure Analysis, 35, pp. 703–712, 2013.
16. M. Oudjene, M. Khelifa, "Elasto-plastic constitutive law for wood behaviour under compressive loadings", Construction and Building Materials, 23 (11), pp. 3359–3366, 2009.
17. M. Oudjene, M. Khelifa, "Experimental and numerical analyses of single double shear dowel-type timber joints", in *WCTE - World Conference on Timber Engineering*, 2010.
18. A. Reiterer, S. E. Stanzl-Tschegg, "Compressive behaviour of softwood under uniaxial loading at different orientations to the grain", Mechanics of Materials, 33 (12), pp. 705–715, 2001.
19. Y. A. Pranata, B. Suryoatmono, "Nonlinear Finite Element Modeling of Red Meranti Compression at an Angle to the Grain", Journal of Engineering and Technological Sciences, 45 (3), pp. 222–240, 2013.
20. C. L. dos Santos, J. J. L. Morais, A. M. P. de Jesus, "Mechanical behaviour of wood T-joints. Experimental and numerical investigation", Frattura ed Integrità Strutturale, 9 (31), pp. 23–37, 2014.
21. Simulia ABAQUS, "User's Guide". 2019.
22. R. J. Ross, F. P. L. USDA Forest Service., "Wood handbook : wood as an engineering material", 2010.
23. R. H. Hemanth *et al.*, "Performance Evaluation of Finite Elements for Analysis of Advanced Hybrid Laminates", in *SIMULIA Customer Conference*, 2010, pp. 1–15.

LIST OF FIGURES AND TABLES:

Rys. 2. (a) DCB – Podwójna belka wspornikowa, (b) ENF – Zginana belka z nacięciem.

Fig. 3. (a) WS – Wedge Splitting sample, (b) K_{Ic} specimen, (c) K_{IIc} specimen.

Rys. 3. (a) WS – Podzielona próbka klinowa, próbka do wyznaczania (a) K_{Ic}, (b) K_{IIc}.

Fig. 4. (a) Oudjene specimen, (b) Santos specimen.

Rys. 4. (a) próbka Oudjene, (b) próbka Santosa.

Fig. 5. Theoretical isolation of the compression and tension zones.

Rys. 5. Teoretyczne wydzielenie strefy ściskanej i rozciąganej.

Fig. 6. Constitutive law for wood used in the model.

Rys. 6. Prawo konstytutywne dla drewna wykorzystane w modelu.

Fig. 7. A typical sample and the laboratory setup.

Rys. 7. Typowa próbka i stanowisko laboratoryjne.

Fig. 8. Denotations for a three point bending test.

Rys. 8. Oznaczenia przy badaniu trójpunktowego zginania.

Fig. 9. Trend lines of the strengths determined based on laboratory tests.

Rys. 9. Linie trendu wytrzymałości wyznaczone na podstawie badań laboratoryjnych.

Fig. 10. Experimental *P/w* curves and its statistical approximations

Rys. 10. Eksperymentalne krzywe *P/w* i ich statystyczne przybliżenia

Fig. 11. Finite element mesh and boundary conditions used in the analyses.

Rys. 11. Siatka elementów skończonych i warunki brzegowe wykorzystane w analizie.

Fig. 12. Comparison of *P/w* relation from FEM model and laboratory tests.

Rys. 12. Porównanie zależności *P/w* z modelu MES i badań laboratoryjnych

Fig. 13. Comparison of forms of destruction from the FEM model and laboratory tests.

Rys. 13. Porównanie form zniszczenia z modelu MES i badań laboratoryjnych.

Table 1. Elastic parameters and strengths of the tested softwood.

Tabela 1. Parametry sprężyste i wytrzymałości badanego drewna.

SYMULACJA 3D ZGINANYCH ELEMENTÓW Z MIĘKKIEGO DREWNA W PROGRAMIE ABAQUS

Słowa kluczowe: MES, Modelowanie Drewna, Miękkie Drewno, Pękanie, Zniszczenie

STRESZCZENIE:

Artykuł przedstawia sposób modelowania elementów zginanych wykonanych z miękkiego drewna. Taki rodzaj drewna jest najczęściej wykorzystywany w konstrukcjach budowlanych. Autorzy wykonali zwięzły przegląd sposobów modelowania drewna na podstawie literatury. Znalazły się w nim trzy podstawowe podejścia: liniowo-sprężysta mechanika pękania (LEFM), mechanika zniszczenia ośrodków ciągłych (CDM) i funkcja Hilla (HF). W pracy zaproponowano rozwiązanie oparte na funkcji Hilla, która dostępna jest w programie ABAQUS. Zróżnicowane zachowanie materiału przy ściskaniu i rozciąganiu osiągnięto poprzez teoretyczny podział modelu na strefę ściskaną

i rozciąganą. W obu strefach przyjęto różną wytrzymałość wzdłuż włókien w zależności od panującego stanu naprężenia. Na podstawie badań laboratoryjnych wprowadzono ogólne zależności pomiędzy parametrami sprężystymi i wytrzymałościowymi. Dzięki temu do zastosowania modelu wystarczające jest obliczenie modułu sprężystości wzdłuż włókien (E_L) i wytrzymałości na rozciąganie przy zginaniu (MOR). Oba parametry można wyznaczyć bezpośrednio w badaniu trójpunktowego zginania. Prawidłowość modelu MES została potwierdzona badaniami laboratoryjnymi oraz metodą cyfrowej korelacji obrazu (DIC). Model umożliwia przewidywanie zachowania elementów z drewna przy zginaniu w stanie 3D. Uwzględnia zarówno plastyczne płynięcie w środkowej fazie obciążenia, spowodowane przekroczeniem wytrzymałości na ściskanie, jak i przewidywanie siły maksymalnej w wyniku rozciągania. Rozwiązanie jest bardzo praktyczne ze względu na brak problemów ze zbieżnością obliczeń. Dodatkowo liczba wymaganych parametrów jest znacznie mniejsza niż w przypadku innych metod odnalezionych w literaturze.

Received: 17.02.2020 Revised: 30.05.2020